OPTIMIZATION OF WATER INJECTION INTO VAPOR-DOMINATED GEOTHERMAL RESERVOIRS*

Roman B. Sta. Maria[1] and Roland N. Horne[2]

1. Philippine Geothermal, Inc. 2. Stanford University

Abstract

Water injection into a vapor-dominated geothermal reservoir is an effective method of sustaining steam production from the field. Injection puts additional water to the reservoir and raises the prevailing reservoir pressure. This process improves the field's productivity. However, the increased pressure also increases the water retention capacity of the reservoir rocks through the effects of adsorption and capillary condensation.

Due to the significant costs associated wirh water injection programs, optimizing injection not only involves maximizing the energy yield fiom the resource but also the present worth of the project. Two crucial parameters that need to be established are: 1) how much to inject; and, 2) when to inject it. This study investigated the optimal design of these parameters.

It was found that comparable energy yield can be attained for injection programs that are initiated at various stages of the field's development. Higher injection rates are desirable when the injection program starts later in the productive life of the field. Considering the economics of the project, it is best to implement the injection program during the later stages of the field's development. This way, a greater fraction of the injectate can become available for production and at the same time optimize the present worth of the project.

INTRODUCTION

The ability to model the effects of water injection into vapor-dominated reservoirs is of great interest to the geothermal industry. Experience has shown that vapor-dominated systems are prone to run out of water even though vast amounts of heat still remain in the reservoir. It has been established through research and field studies that water injection into the reservoir can provide artificial mass recharge to improve steam production from the field (Enedy et al, 1991). However, if done incorrectly, injection may have detrimental effects on production (Barker et al., 1991). Clearly, an appropriate injection program is a major component of resource management strategy for vapor-dominated geothermal reservoirs.

Adsorption and capillary pressure are major factors affecting the behavior of vapor-dominated geothermal reservoirs. These mechanisms affect both the estimation of the reserves and the production performance of the field. The effectiveness of water injection programs to sustain the field's productivity is also affected. Hence the optimization of an injection strategy should include consideration of these effects.

Physical adsorption is the phenomenon by which molecules of steam adhere to the surfaces of a porous medium. This phenomenon is caused mainly by Van der Waals forces. When sufficient deposition has taken place, a capillary interface may form and deposition due to capillary condensation becomes more significant (Home et al., 1995). In addition, the surface between the vapor and the liquid phases in a porous medium is not flat. It is a well-recognized phenomenon that the vapor pressure above the curved surface of a liquid is a function of the curvature of the liquid-vapor interface. Thus, curved interface thermodynamics is more appropriate than flat interface thermodynamics. The curvature of the surface gives rise to vapor pressure lowering (VPL), thus allowing liquid and vapor to coexist in equilibrium at pressures that are less than the saturation pressure.

* Reprinted by permission of the Geothermal Resources Council.

Understanding how adsorption and capillary forces affect water injection is particularly relevant at this time because of the plans to increase water injection into The Geysers geothermal field. Although water injection has been ongoing for many years, injection rates will increase significantly when water from Lake County, and possibly the city of Santa Rosa, becomes available for injection.

Numerical simulation is an effective method to forecast the performance of a geothermal reservoir. Until recently, simulators have used flat interface thermodynamics to define the phase of the reservoir. However, the development of new simulation codes has enabled the effects of adsorption and curved interface thermodynamics to be incorporated. This study made use of these simulators to investigate of the effects of adsorption and capillary pressure on water injection into geothermal reservoirs. The ultimate objective is to optimize water injection into a hypothetical vapor-dominated geothermal field.

PRELIMINARY WORK

The simulator TETRAD was used in this study. TETRAD is a commercial simulator that has been modified to account for vapor pressure lowering (VPL). Version 12 of this simulation code uses the generalized vapor pressure lowering algorithm developed in the Idaho National Engineering Laboratory (Shook, **1993).** This algorithm follows-up on an earlier work by Holt and Pingol (1992) to modify the standard steam tables to account for vapor pressure lowering.

The data required to incorporate vapor pressure lowering in numerical simulations is either a capillary pressure relationship (p_c versus S_w) or an adsorption isotherm. TETRAD requires a p_c versus S_w relationship like the one shown in Figure 1.

This capillary pressure relationship was based on the adsorption isotherm shown in Figure 2. The two sets of data are equivalent and conversion from one to the other is done through the Kelvin equation and an intermediate relation for X vs. S_w. For more details, refer to the paper by Sta. Maria and Pingol (1**996).**

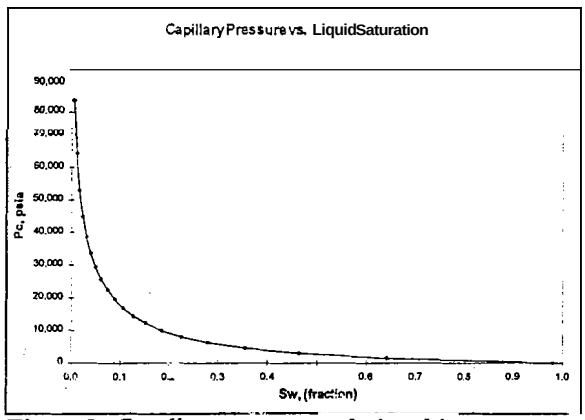

Figure 1: Capillary pressure relationship.

THE RESERVOIR MODELS

Two vapor-dominated reservoir models (with simple geometry) were developed to investigate the effects of adsorption and capillarity on injection. The geometry of these models are illustrated in Figure **3** and Figure 4. The basic properties used in both models are listed in Table 1. The relative permeability function used causes steam to be the only mobile phase at the given initial water saturation. Water becomes mobile when S_w is greater than 35%. Adsorption properties are patterned after those typically observed in The Geysers.

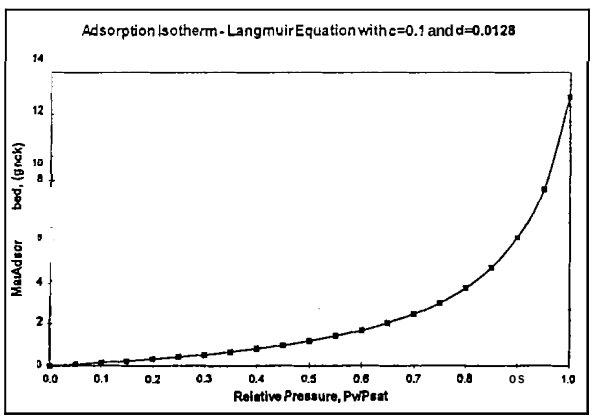

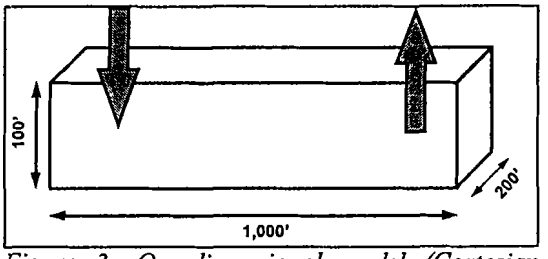

Figure 3: One-dimensional model (Cartesian

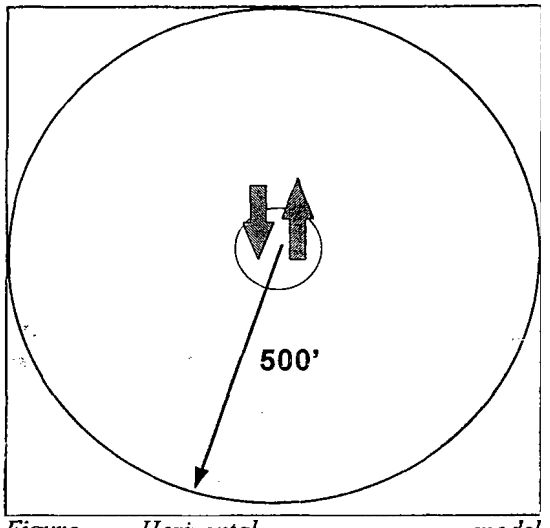

Figure Horizontal model (radial

Porosity	5%
Permeability	20 md
Initial liquid saturation	30%
Initial reservoir pressure	400 psia
Reservoir temperature	Evaluated

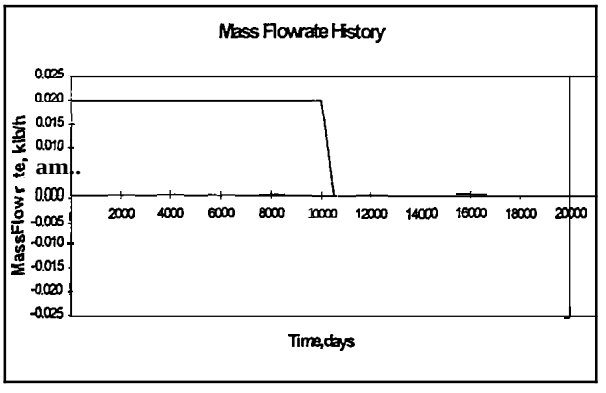

The reservoir was perturbed by injecting cold water (90 °F). Figure ***5*** shows that 20 lbs/h of water is injected during the first 10,000 days. Afterwards, the field was shut-in and the reservoir allowed to equilibrate.

Figures ***6, 7,*** and **8** contrast the behavior of the reservoir **if** it is modeled with and without adsorption and vapor pressure lowering. Shown in these plots are the reservoir pressure, reservoir temperature, and phase saturation measured in the injection gridblock.

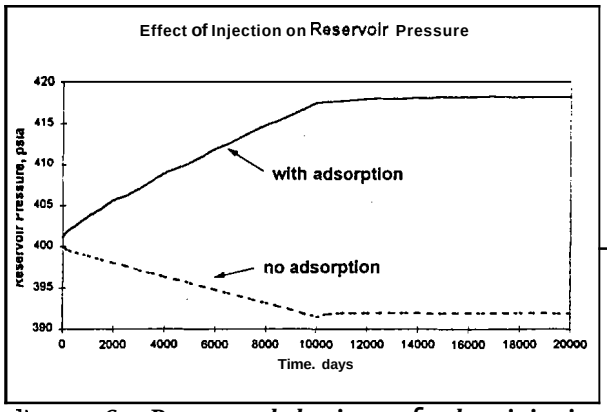

Figure 6: Pressure behaviors of the injection gridblock.

Figure *6* shows the reservoir pressure through time. With no adsorption the pressure measured in the injection gridblock is observed to decline. With adsorption the opposite effect is observed. Instead of declining, the pressure is observed to rise in response to injection.

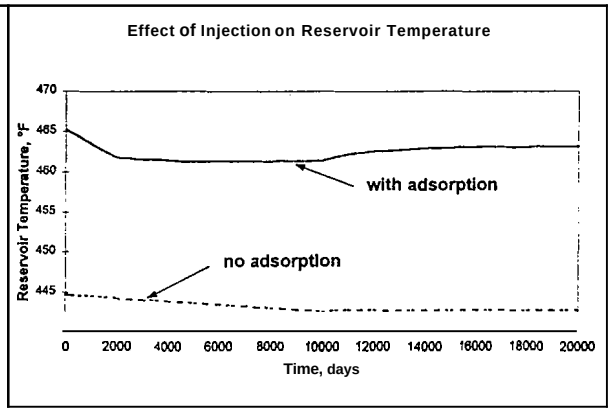

***Figure** 7: Temperature behaviors of the injection gridblock.*

Figure 7 shows the reservoir temperature through time. As mentioned earlier, the use of pressure as the independent parameter to specify the thermodynamic state of the reservoir result in different temperatures for models with and without vapor pressure lowering. Without adsorption, the reservoir temperature is about 445 °F; this is the saturation temperature at 400 psia if the vapor/liquid interface is flat. With vapor pressure lowering, 400 psia actually corresponds to a lowered vapor pressure across a curved vapor/liquid interface. With the water saturation initially at 30%, the given adsorption isotherm dictate. the appropriate reservoir temperature to be about 465 °F. Thus, in terms of initial energy in-place the models with and without adsorption are not equivalent. The differences are not limited to the heat in-place but also on the temperature variation of each gridblocks. Without adsorption, temperature declines monotonically for all gridblocks. With adsorption, the gridblocks adjacent to the injection gridblock initially exhibit increasing temperature before starting to decline (not shown in Figure 7).

A curious behavior of the reservoir pressure is illustrate? below. Shown in Figure 8 are the reservoir pressures measured in the injection and production gridblocks through time. The pressure in the injection gridblock was initially higher than the production gridblock. However, after 4,000 days the situation is reversed; the production gridblock have higher pressure than the injection gridblock. However, throughout the entire injection period there is a net mass flowing away from the injection gridblock towards the production gridblock.

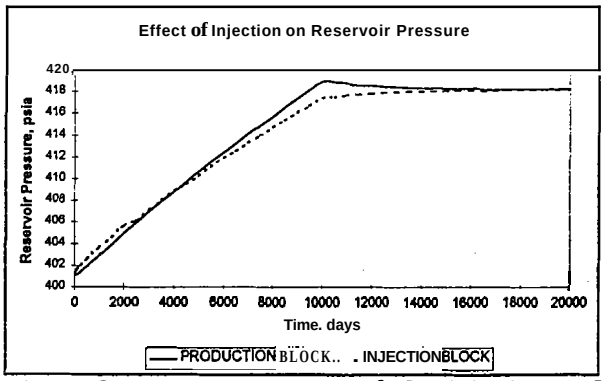

Figure 8: Pressure response of the injection and production gridblocks.

The apparent contradiction in pressure gradient and mass flow is explained by keeping in mind that the pressure of the vapor and liquid phases are different. As defined earlier, the reservoir pressure shown in Figure 8 is the pressure of the vapor phase. Thus, initially steam is migrating away from the injection gridblock. At a later time, the pressure gradient is reversed and steam migrates towards the injection gridblock. On the other hand, water will continuously move away from the injection gridblock towards the production gridblock.

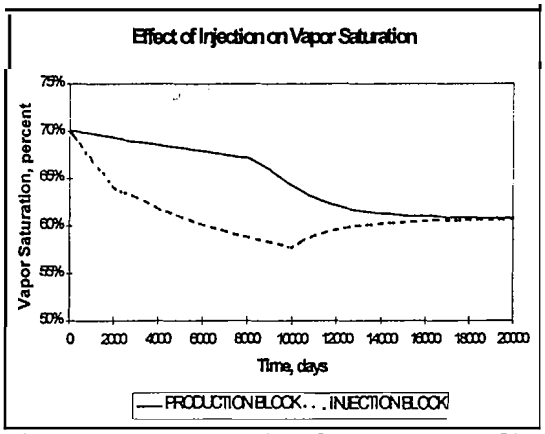

Figure 9: Vapor saturation changes measured in the injection and production gridblocks.

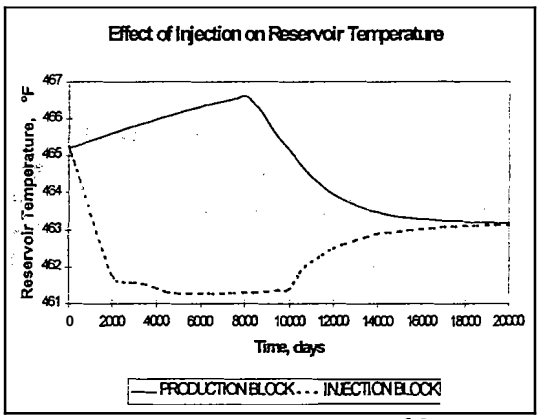

Figure 10: Temperature responses of the injection and production gridblocks.

The pressure of the water phase is always higher in the injection gridblock than the production gridblock, or any other adjacent gridblocks. This can be explained if we consider the saturation variation between gridblocks as shown in Figure 9. The vapor saturation of the injection gridblock is less than the production gridblock. From Figure 1 we know that the capillary pressure increases as the vapor saturation increases (i.e., decreasing liquid water saturation). Capillary imbibition draws water from the injection area towards the production area. Even though there is a counter-flow of steam and water, the net mass flow is still directed away from the injection area.

To complete the picture, Figure 10 shows the reservoir temperature measured in the injection and production gridblocks.

The next step was to use the two-dimensional radial model to investigate the behavior of the reservoir when we try to produce the injected water. To do this, we imposed adsorption and vapor pressure lowering on the model. During water injection, the reservoir pressure is raised above the initial reservoir pressure. After terminating injection, the production well was opened. Production is constrained such that the maximum production rate does not exceed the injection rate and the well is able to produce only down to the point when the reservoir pressure is restored to its initial value.

Figure 11 shows the reservoir pressure throughout the 30,000 days simulation period. There was constant rate injection from 5,000 to 10,000 days. The production well is opened beginning at 15,000 days. The well is allowed to produce as long as it can sustain production based on the given constraints.

Figure 12 shows the resulting mass flowrate history of the model. We used a sign convention such that injection is denoted by a positive mass flow while production is denoted by negative mass flow. It is apparent from the plot below that the production rate declines rapidly in response to the decline of the reservoir pressure.

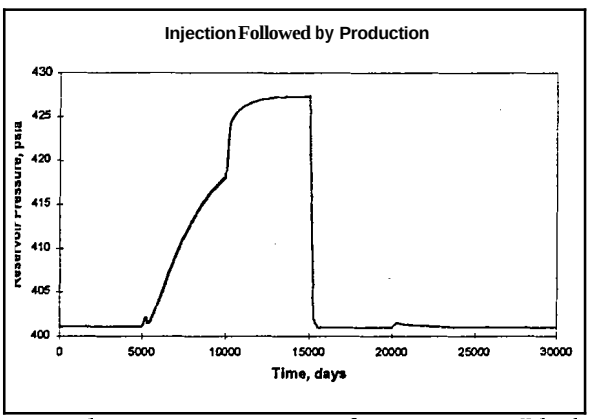

Figure 11: Pressure behavior of the central gridblock in response to injection followed by production.

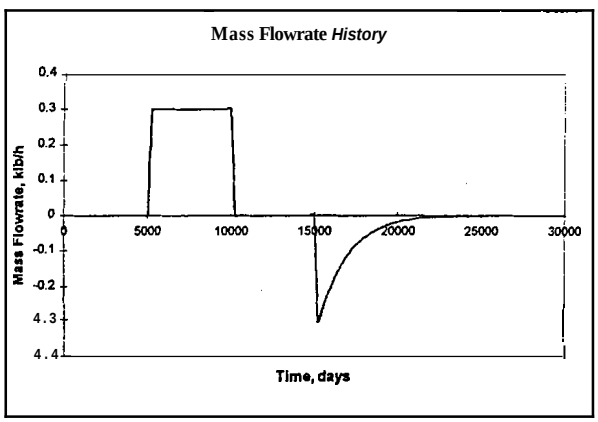

Figure 12: Production and injection history.

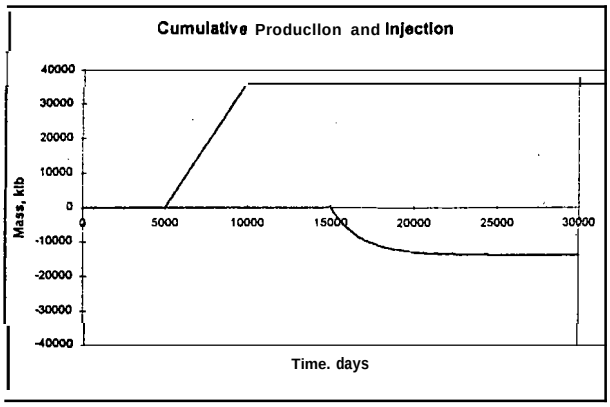

Figure 13 shows the same information as the previous plot but in terms of cumulative production and injection through time. The total mass injected into the reservoir is 36×10^6 lbs. The total mass produced afterwards is about 13.82×10^6 lbs. The total mass produced amounts to only **38.4%** of the mass injected. The mass difference of over 22×10^6 lbs is retained in the reservoir and will be produced only if the reservoir pressure is allowed to decline below 400 psia.

***Figure 13:** Cumulative masses produced and injected*

OPTIMIZATION OF INJECTION

A field-scale model of a geothermal reservoir is necessary to study the optimization of water injection projects. The objective of this study is to determine the appropriate injection strategy that would result to an optimum energy yield from the geothermal resource while maximizing the net present worth of the injection project. There are *two* main questions what will be addressed in this study. How much water to inject and when to start injecting?

The Reservoir Model

A field-scale model of a hypothetical vapor-dominated geothermal reservoir was developed. The lateral extent of the reservoir is arbitrarily defined to be 7,000 feet by 7,000 feet. The vertical extent of the reservoir is 7,200 feet. The top of the reservoir is located at 2,000 feet below the ground surface. The basic properties of the reservoir model are listed on Table 2 below.

*Table 2: **Reservoir properties of the full-field model.***

Porosity	5%
Lateral permeability	40.008 md
Vertical permeability	20.004 md
Initial liquid saturation	35%
Initial reservoir pressure	400 psia
Reservoir temperature	Evaluated

Single porosity formaiation was used to construct the reservoir model. Comparison of models constructed using single and dual porosity formulations shows that there is no significant difference in model performance during production. For the dual porosity model, it was assumed that the fractures also have adsorption properties identical to the matrix. This was a necessary assumption to have an initial mass in-place in the dual porosity model that was equal to that of the single porosity model. Another reason is to enable the use of curved interface thermodynamics in both the matrix and fracture gridblocks. However, the issue of how fractures should be treated with respect to adsorption property is still unknown question. Therefore, single porosity formulation was used to simplify the model and avoid the complications associated with the dual porosity formulation.

The lateral permeability value of 40.008 md given in Table 2 is equivalent to that of a fractured system with a matrix permeability of 0.01 md (4% bulk porosity) and a fracture permeability of 200 md (1% bulk porosity). The vertical permeability was arbitrarily defined as 50% of the lateral permeability.

The relative permeability functions used were based of the work of Sorey (1980). The liquid and vapor permeability functions are defined as follows:

$$k_{rl} = S_w^{*4}$$
$$k_{rv} = (1-S_w^{*2})(1-S_w^{*})^2$$
where $S_w^{*} = (S_w-S_{wc})/(1-S_{wc})$ and $S_{wc} = 0.35$

Because the initial liquid saturation of the reservoir was set to 35%, only the steam phase is mobile initially. The liquid phase can become available for production by evaporation or if it becomes mobile when the liquid saturation rise above 35% through steam condensation or influx of additional water through injection.

Similar to the previous evaluation models, the field-scale model is essentially a closed tank. The model boundaries are closed to heat and mass flows. The only way heat and mass can flow to and from the reservoirs is through the production and injection wells.

The Field Model

The installed generating capacity of the field is 75 MW(e). Assuming a plant capacity factor of 90%, the average gross generating capacity of the field is 67.5 MW(e). The steam usage is 18.5 klbh per MW(e). Thus, the required average production rate from the field to sustain full generating capacity is about 1,250 klbh. It was assumed that a minimum flowing bottomhole pressure of 100 psia is required to deliver steam to the power plant.

The field is located at an elevation of 2,000 feet above the source of water for injection. All injection water will be coming from this source. A 10-mile pipeline brings water from the lowland source to the geothermal field.

Injection Optimization Scheme

Instead of modeling the entire reservoir, a symmetry element 1/50 the size of the reservoir is modeled. This symmetry element have dimensions of 1,400 feet ***by*** 1,400 feet laterally and 3,600 feet thick. If the full-scale reservoir is gridded into 5×5×2 layers, one gridblock will be represented by the symmetry element.

The symmetry element was further gridded into 7×7×9 layers. Each gridblock have dimensions of 200-by-200 feet and 400 feet thick. A pair of production and injection well are placed on diagonally opposite comers of the element. The injection well was completed in layer 5. The production well was completed in layers 4, 5, and ***6***. An observation well is placed in the center of the element and completed in layer 5. This production **and** injection wells placements implies that the field was developed with a five-spot pattern. All subsequent measurements of the reservoir properties were conducted in layer 5.

Assuming that mass is produced uniformly throughout the reservoir, the field's total average production rate of 1,250 klb/h translates to a production rate of 25 klb/h for each symmetry element. For all subsequent simulation runs, the production rate of 25 klbh will be referred to as the peak production rate. The water injection rates will be scaled relative to this peak production rate.

To investigate the issue of when should injection begin during the field's development, seven cases were considered. For all of these cases, production begins at time t=O years while the injection operation begins at various stages of the field's exploitation. The cases considered are the following (Cases 1-VII):

Case I: Injection begins at t = 0 year;
Case 11: Injection begins at t = ***5*** years;
Case III: Injection begins at t = 10 years;
Case IV: Injection begins at t = 15 years;
Case V: Injection begins at t = 20 years;
Case VI: Injection begins at t = 25 years; and,
Case VII: Injection begins at t = 30 years.

For each of the cases above, the effects of injecting water at different rates were further investigated. These sub-cases are the following (Cases A- H):

Case **A:** Base case - no injection;
Case B: Inject 20% of the peak production rate;
Case C: Inject 40% of the peak production rate;
Case D: Inject 60% of the peak production rate;
Case E: Inject 80% of the peak production rate;
Case F: Inject 100% of the peak production rate;
Case G: Inject 120% of the peak production rate;
Case H: Optimum case - injection rate causing water breakthrough at t = 50 years.

The cases described above required a total of 50 permutations. The optimum case (Case H) uses water breakthrough in the production well at t = 50 years (18,250 days) as the optimization criteria. The optimum rate may be less than or greater than the rate used in Case G (120% of peak rate).

Results

The first simulation performed was intended to establish the base case production performance of the reservoir. The production well was opened at t = 0 days and allowed to flow for 50,000 days. The production rate was constrained to a maximum rate of 25 klbs/h. The production well's bottomhole flowing pressure was constrained to a minimum of 100 psia. The base case production performance (first 20,000 days) is illustrated in Figures 14, and 15.

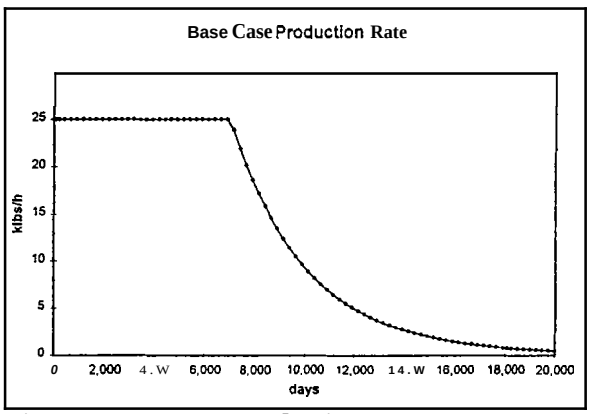

Figure 14: Base case production rate.

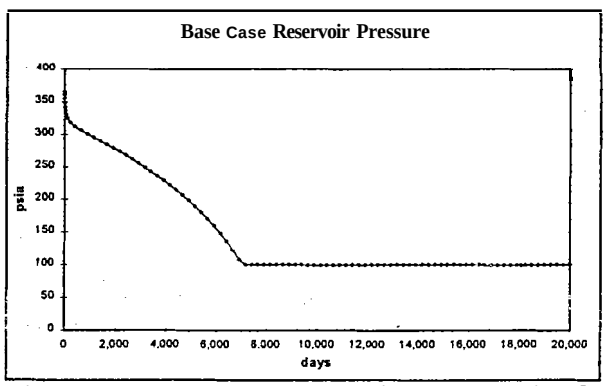

Figure 15: Base case reservoir pressure in the production gridblock.

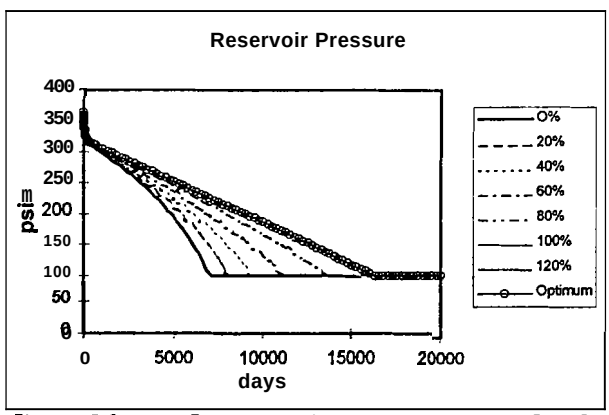

Figure 16: Case I - Reservoir pressure measured at the production gridblock.

Figure 14 shows that the reservoir can sustain peak production rate for about 7,000 days, or 19 years. After 19 years, the steam production rate declines exponentially with a nominal rate of about 0.12 per year.

Figure 15 below shows the reservoir pressure measured in the production gridblock through time. After a rapid drawdown, the reservoir pressure declined gradually as steam from the neighboring areas migrate into the production area. The bottomhole pressure constraint of 100 psia was reached after 19 years of production.

To illustrate the production optimization process, shown in the following plots are results for Case I. In this case, injection and production begins at the same time at t = 0 years.

Figure **16** and Figure **17** are plots of the reservoir pressures through time measured in the production and observation gridblocks, respectively. In this case, the optimum injection rate is **93%** of the peak production rate. It is clear from these plots that higher injection rates provide greater support to the reservoir piessure.

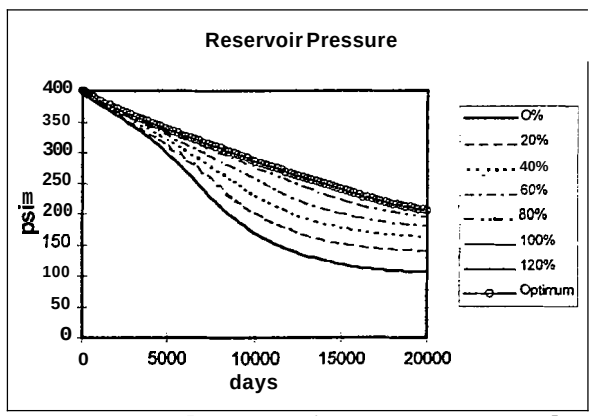

Figure 17: Case I - Reservoir pressures measured at the observation gridblock.

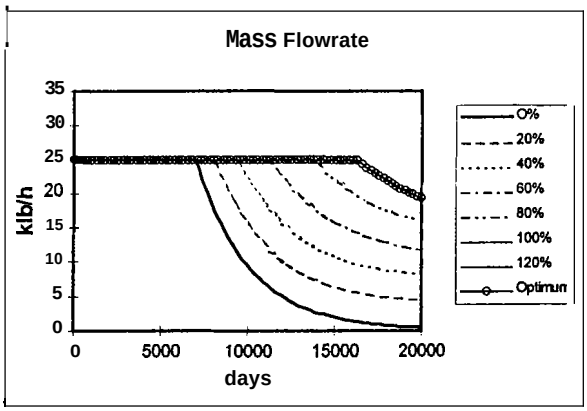

Figure 18: Case I - Steam production rates.

Pressure support from injection translates to increased deliverability. Figure 18 shows that the steam production rate of 25 klb/h can be sustained much longer than the base case. Thus, cumulative production is also increased. This is shown in Figure 19.

As mentioned earlier, the criteria used to determine the optimum injection rate is the onset of water breakthrough in the production well at the 50th year. Figure 20 shows the water production rates for various injection rates of Case I. Injecting 100% and 120% of the peak production rate caused early breakthroughs. Injecting 93% of the peak rate satisfied the optimum criteria. Injecting water with a higher rate will cause water to breakthrough before the 50th year.

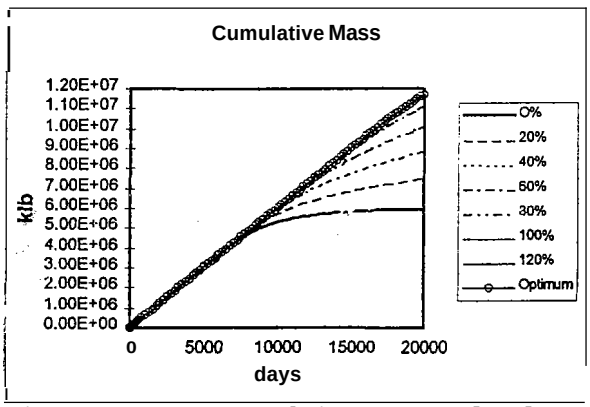

Figure 19: Case I - Cumulative masses produced.

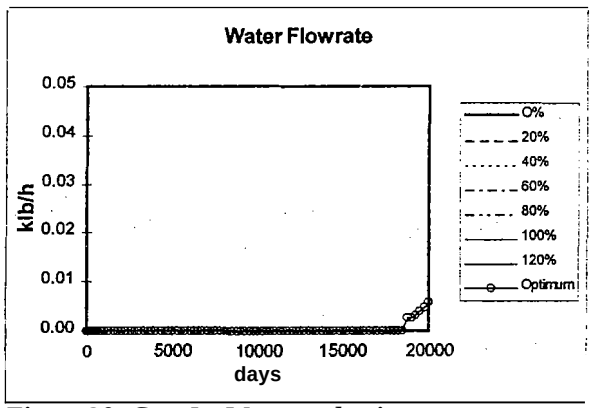

Figure 20: Case I - Water production rates.

The optimum injection rates for all seven cases are shown graphically in Figure 21. There is a clear trend that starting water injection later in the field's development results to higher allowable injection rates. For example, Case VII where injection started in the 30th year of production, the optimum injection rate is 224% of the peak production rate.

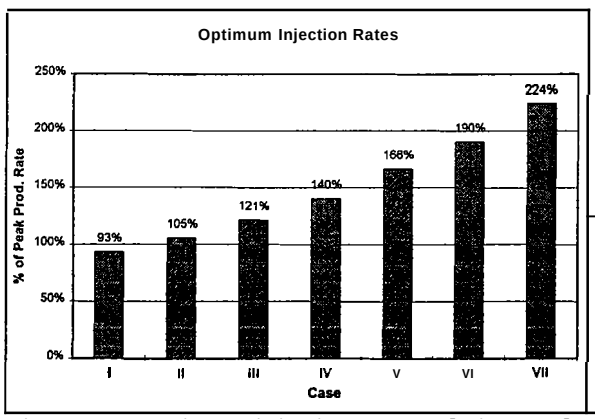

Figure 21: Optimum injection rates relative to the peak production rate.

Another interesting parameter is how much of the injected water is eventually produced. Injectate recovery is defined as incremental mass produced

The resulting optimum incremental production for each of the cases are shown in Figure 22. Except for Case VI and Case VII, the optimum incremental production exceed 80% of the base case. The lower incremental production of cases VI and VII are mainly due to the limited production period after injection.

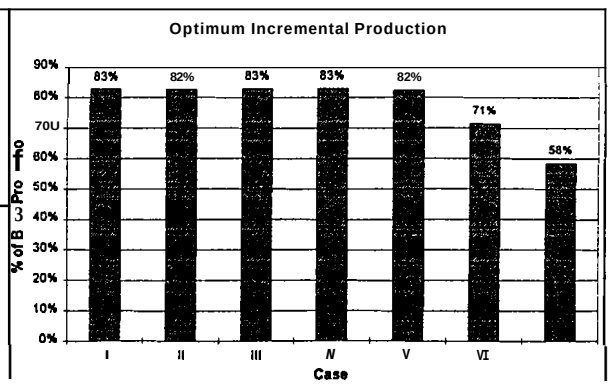

Figure 22: Optimum incremental production relative to the base production.

(with injection) divided by the base case production. The injectate recoveries for all the cases are shown in Figure 23. It **is** clear from this graph that injection recoveries are lower for higher injection rates. In Case lV, injecting 20% (Sub-case B) results to a recovery of about 57%. Injecting 120% (Sub-case G) have a recovery of 48%. For the optimum case (Sub-case H), injecting 140% results to a recovery of only about 46%.

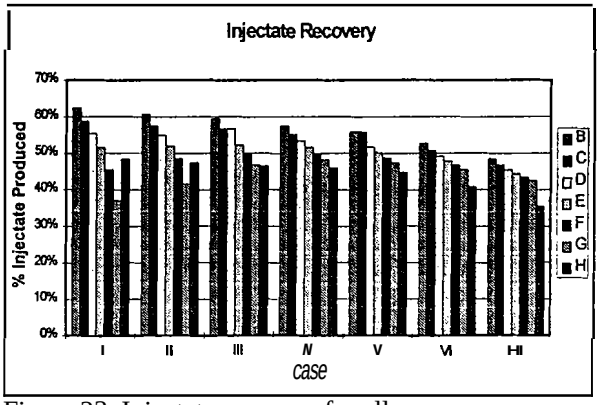

Figure 23: Injectate recovery for all cases.

Economic Optimum

Several assumptions were made about the field model and these were used to construct an economic model. We used this economic model to determine which of the cases previously considered yields the maximum present worth. Only the incremental costs and benefits of the injection project were considered because the costs and benefits associated with the base case are common to all the cases.

Incremental steam production is converted to incremental generation using the steam rate of 18.5 klb per MWh (net). The gross income from this incremental generation is evaluated using an assumed income of $25 per MWh. Using the cash flow method, a discount rate of 10% per year was used to account for the time value of money.

As mentioned earlier, the field **is** located at an elevstion of 2,000 feet above the water source. All injection water will come from this source through a 10-mile water pipeline. These information were used to evaluate the capital expense required to build the pipeline and the pumping facilities. Building the pipeline costs $12 per diameter inch-feet installed. The pump's capital cost is $1,341/kW ($1,000/hp). The needed structures. controls, and power supply **for** the pump costs $2,682/kW ($2,000/hp).

For the full-field injection rates ranging from 250 klb/h (20%) to 3,000 klb/h (240% of peak rate), the combination of pump and pipeline sizes were optimized with the objective of minimizing the required capital expense for a given injection rate. With a choice of using either a ***6,*** 12, 18, 24, or 30 inches diameter pipe, the power needed to pump water to the required elevation and also account for frictional pressure drop in the pipeline was evaluated ana optimized. The optimum cases are given in Table 3. The total capital cost shown (pumping facilities and pipeline) is scaled to the size of the symmetry element (1/50 of the whole field).

Table 3: Optimum pump and pipeline facilities.

% Injection	Pipe *Size* (Inches)	Pump **Power (kW)**	Capital **cost (k$)**
20%	6	285	99
40%	6	1.132	167
80%	12	942	228
100%	12	1,308	257
120%	**12**	1,762	294
140%	**12**	**2,318**	**339**
160%	**18**	1,704	365
180%	18	1.975	**387**
200%	18	2,267	411
220%	18	2,582	436
240%	18	2.922	463

There are two other information required to complete the economic model; operating cost of the injection system, and cost of the water injection wells. The cost of the pipelines to distribute water to the injection wells was ignored.

The operating cost was estimated as a function of the total mass of injected water. By making assumptions on the cost of electricity to operate the pumps, the operating cost function **of** $0.1 **1** per klb of water was used.

It was also assumed that a total of six injection wells is required to develop the field. If the average cost of drilling a well is $1.5 million, the total cost for the injection wells is $9 million. Scaling to the symmetry element (1/50), the cost of the injection well attributed to the symmetry element is $180,000.

A cash flow was generated for each of the cases considered previously. The net present worth of the injection project was evaluated using the assumed discount rate. Figure 24 below shows the graph of the present worth of all the cases.

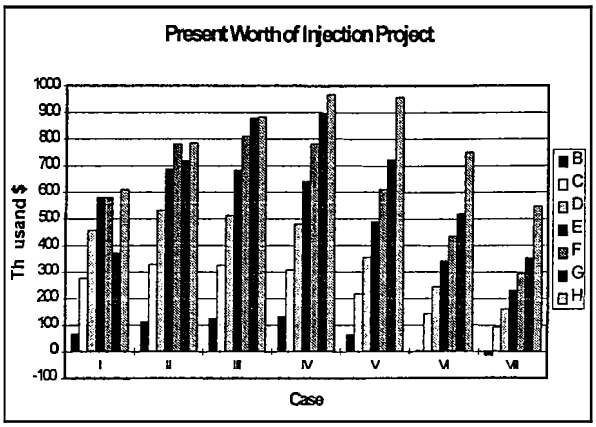

Figure 24: Present worth of injection project for all cases.

For all cases, the optimum injection rates (Case H) gives the maximum present worth for that particular case. Comparing all the cases, the optimum present worth is $966,000 for Case IV. This is followed closely by Case V with $956,000. For Case IV and Case V, the injection started at the 15th and 20th year, respectively. Most likely, the real optimum occurs when injection starts between 15 and 20 years of the field's operation. Injecting earlier than the 15th year requires capital expenditure that are sooner than necessary. Injecting later than the 20th year requires higher injection rates; thus, higher capital expenditures. Furthermore, there will be loss of opportunity to produce at peak rate because production from the field starts to decline after 19 years.

The cases discussed in this paper ai-e all hypothetical. Therefore, the models and forecasts are not directly applicable to real fields. However, the same optimization process can be applied to a real field to assist in the development of an appropriate injection program.

CONCLUSIONS

This study shows that adsorption and capillary pressure are major factors governing the behavior of vapor-dominated geothermal reservoirs. These mechanisms affect both the resource size estimation and the production performance of the field.

The effectiveness of water injection programs to sustain the geothermal field's productivity is affected by adsorption and capillary pressure. Water injection into vapor-dominated reservoirs provides pressure support and mass recharge to the reservoir. Although this improves productivity, it also increases water retention in the reservoir through adsorption and capillary condensation.

Comparable mass and energy yield can be attained for injection programs starting at various stages of the field's exploitation. Higher injection rates are desirable when injection starts later in the life of the project. From the perspective of economics, an injection program intended to sustain the productivity of the reservoir is best implemented during the later stages of the field's productive life. This way, a greater fraction of the water injected becomes available for production yet optimizing the benefits of the time value of money.

ACKNOWLEDGMENTS

This work was supported by the U.S. Department of Energy, Geothermal Division, under contract DE-FG07-90ID12934 and DE-FG07-95ID13370, through the Stanford Geothermal Program. Permission to publish this paper were granted by Stanford University, Unocal Corporation, and Philippine Geothermal, Inc.. Permission to republish was graciously given by the Geothermal Resources Council.

REFERENCES

Holt, R., and Pingol, A., "Adding Adsorption to a Geothermal Simulator", Proc. of the 17th Annual Workshop on Geothermal Reservoir Engineering, Stanford University, California, January 1992.

Home, R., Ramey, H. Jr., Shang, S., Correa, A., and Hornbrook, J., "The Effects of Adsorption and Desorption on Production and Reinjection in Vapor-Dominated Geothermal Fields", Proc. of the World Geothermal Congress 1995, Florence, Italy, May 1995, pp. 1973-77.

Hsieh, C.H., and Ramey, H.J. Jr., "Vapor-Pressure Lowering in Geothermal Systems", Society of Petroleum Engineers Journal, February 1983.

Lim, K-T., "Simulation of Fractured Reservoir with Sorption and Applications to Geothermal Reservoir", PhD thesis, Stanford University, California, March 1995.

Pruess, K., and O'Sullivan M., "Effects of Capillarity and Vapor Adsorption in the Depletion of Vapor-Dominated Geothermal Reservoirs", Proc. of the 17th Annual Workshop on Geothermal Reservoir Engineering, Stanford University, California, January 1992.

Pruess, K., "Numerical Simulation of Water Injection into Vapor-Dominated Reservoirs", ", Proc. of the World Geothermal Congress 1995, Florence, Italy, May 1995, pp. 1673-79.

Shang, S., Home, R., and Ramey, H. Jr., "Experimental Study of Water Adsorption On Geysers Reservoir Rocks", Proc. of the 18th Annual Workshop on Geothermal Reservoir Engineering, Stanford University, California, January 1993.

Shook, M., "Generalization of Vapor Pressure Lowering Effects in an Existing Geothermal Simulator", Idaho National Engineering Laboratory Report, Idaho, June 1993.

Shook, M., "Effects of Adsorption on Exploitation of Geothermal Reservoirs", Geothermal Resource Council TRANSACTIONS, Vol. 18, October 1994.

Sta.Maria, R., and Pingol, A., "Simulating the Effects of Adsorption and Capillary Forces in Geothermal Reservoirs", Proc. of the 21st Annual Workshop on Geothermal Reservoir Engineering, Stanford University, January 1996.